TITLE
ASP Conference Series, Vol. **VOLUME**, **PUBLICATION YEAR**
EDITORS

Jets in the Solar Tachocline as Diagnostics of Global MHD Processes

J. Christensen-Dalsgaard[1,2], T. Corbard[3], M. Dikpati[2], P.A. Gilman[2], M. J. Thompson[4,2]

[1]*Department of Physics and Astronomy, University of Aarhus, DK-8000, Aarhus C, Denmark*

[2]*High Altitude Observatory, National Center for Atmospheric Research[5], 3450 Mitchell Lane, Boulder, Colorado 80301*

[3]*Observatoire de la Côte d'Azur, Laboratoire Cassiopée, B.P. 4229, F-06304, Nice, France*

[4]*Dept. of Applied Mathematics, University of Sheffield, Sheffield, UK*

Abstract. Multiple theories predict the existence of prograde fluid jets in the solar tachocline. We find helioseismic evidence of a prograde jet near 60° latitude in N and S hemispheres that persists through almost all of the current solar cycle. This evidence favors a hydrodynamic origin for the jet, from global instability of the differential rotation of the tachocline. We see no evidence for jets that migrate toward the equator with the advancing solar cycle, which tends to rule out jets associated with toroidal field bands in the tachocline.

1. Introduction

There are at least two reasons why we might expect to find prograde fluid jets in the solar tachocline. One is that such a jet can contribute to an equilibrium of forces in latitude, between a poleward magnetic curvature stress associated with a band of toroidal field, an equatorward Coriolis force from a prograde fluid jet inside the toroidal band, and an equatorward hydrostatic pressure gradient arising from extra mass placed on the poleward side of the toroidal band (Rempel & Dikpati 2003, and earlier references cited there). A second reason is that the ∼2D (longitude-latitude) instability of the tachocline differential rotation, or a combination of this differential rotation and a coexisting toroidal field, can result in transport of angular momentum by Reynolds and/or Maxwell stresses from low latitudes to a narrow band of high latitudes, thereby spinning the high latitude band up (Gilman & Fox 1997; Charbonneau, Dikpati & Gilman 1999; Dikpati & Gilman 2001a).

[5]The National Center for Atmospheric Research is sponsored by the National Science Foundation.

If helioseismic analysis can reveal the presence of such jets, it may be possible to infer something about the global hydrodynamical and/or magneto-hydrodynamical (MHD) properties of the tachocline. Hence we have undertaken the task of looking for such jets. If the jets are closely tied to the tachocline toroidal fields, then as a solar cycle advances we should expect to see such jets migrate toward the equator. On the other hand, if the jet arises from purely hydrodynamic processes, then it is more likely to be stationary in latitude, though it might not be present at all phases of a solar cycle.

2. Physics of jet sources

2.1. Jets from latitude force balance

As discussed by Rempel and Dikpati (2003, and references therein), a band of toroidal fields in the tachocline can be in latitudinal force balance if there is a prograde toroidal jet inside it of sufficient amplitude. Dikpati and Gilman (2001b) had previously shown that equilibrium can also be attained if there is enough additional mass on the poleward side of the toroidal ring, causing a sufficient equatorward hydrostatic pressure gradient. The sun might choose any combination of these limits, as discussed by Rempel and Dikpati (2003). For toroidal bands of amplitude of solar interest, the angular velocity of the jet relative to the background differential rotation can be expressed as

$$\omega_j \approx \frac{(1-\varepsilon){\alpha_0}^2}{2(\omega_c+\omega_s)} ; \tag{1}$$

here ω_j represents the jet-like toroidal flow, ω_c the core-rotation rate, ω_s the solar-like differential rotation, $\alpha_0\,(1-\mu^2)^{1/2}$ the toroidal field and ε the jet parameter, such that $\varepsilon = 1$ represents no jet and $\varepsilon = 0$ the full jet.

We see from Equation (1) that the magnitude of the jet is proportional to the square of the toroidal field strength. If the force balance is achieved even partially by the Coriolis force associated with the jet this means that the jet is much more likely to be observed if the toroidal field is large. Figure 1 shows graphically the relation between jet and peak toroidal field amplitude, for various latitude positions of the toroidal band, assuming that there is no latitudinal hydrostatic pressure gradient contributing to the force balance. The top and right hand scales are in dimensional units convenient for comparison with solar values. The results are essentially identical for bands of 10° and 20° latitude width.

Several features of Figure 1 are of interest. Clearly the higher the latitude of a band of a given strength, the larger the jet needed to balance the curvature stress. This is because the component of the curvature stress that is directed poleward is larger. In addition, the jet amplitude in nHz that is associated with toroidal bands of peak strength $\sim$100kG, thought to be necessary to produce spots that emerge in low latitudes, is large: even at 15° latitude, a 100kG field would have a jet of $>$ 50nHz, compared to the average interior solar rotation of about 440nHz. Unless the jet is very narrow in latitude and/or radius, this should be detectable by helioseismic methods. And jets at higher latitudes for the same peak toroidal field are even larger.

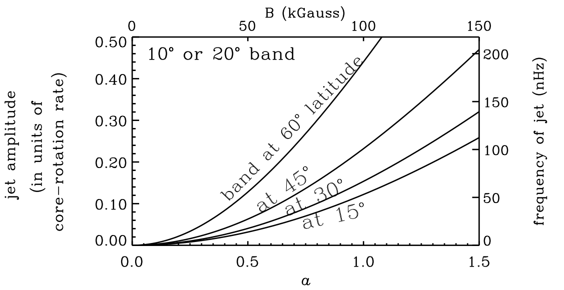

Figure 1. Jet amplitude as a function of peak field strength of a toroidal band placed at different latitudes.

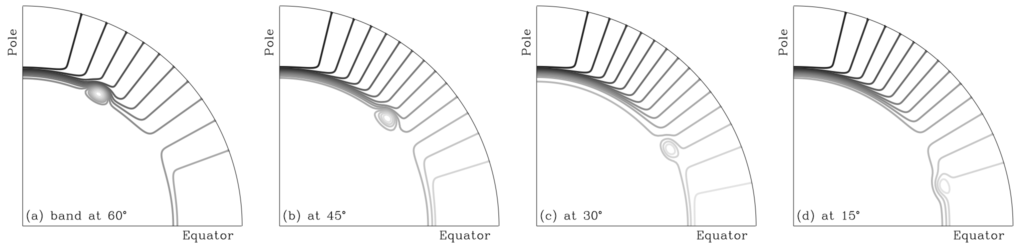

Figure 2. Total internal rotation including background and jet for a 10° band with 60 kG peak field, assuming that balance is entirely between magnetic curvature stress and Coriolis force.

To illustrate how this jet perturbs the rotation contours for an idealized form of the rotation of the convection zone and tachocline, we plot in Figure 2 the sum of background differential rotation and a jet associated with a 60kG toroidal band (gaussian profile) of 10° latitude width (full width at half maximum), for selected latitude positions. This jet is confined to the tachocline depths. This plot illustrates the latitudinal and radial resolution needed to detect such a jet.

In the discussion above we have not addressed the question of how the establishment of the equilibrium among the three forces is achieved dynamically. To our knowledge, there is currently no MHD dynamo model with hydrodynamics included that simulates that process in detail, as a toroidal field is built up. But it is intuitively clear that establishment of a toroidal ring whose poleward curvature stress is initially unbalanced can result in the slippage of that ring toward the poles with an accompanying spin-up of the fluid ring inside it. Whether this actually occurs in the sun is unknown.

2.2. Jets from global HD and/or MHD instabilities

In general, global instabilities of differential rotation in rotating objects such as stars or planets lead to the formation of jets, particularly if the angular momentum extracted from the differential rotation over some range of latitudes is deposited by the unstable modes in a narrow range of other latitudes. These instabilities are usually 2D (longitude-latitude) or nearly so. Instabilities of this type have been explored extensively for the solar tachocline, in the MHD case starting with Gilman and Fox (1997), and in the hydrodynamical case with

Charbonneau, Dikpati and Gilman (1999). The governing equation for initial changes in the differential rotation for both hydrodynamical and MHD cases is given by equation (15) of Gilman and Fox (1997), which we repeat here as

$$\frac{\partial \omega_0}{\partial t} = \frac{1}{(1-\mu^2)} \frac{\partial}{\partial \mu} \left[(1-\mu^2)(\overline{a'b'} - \overline{u'v'}) \right] , \tag{2}$$

in which $\mu = \sin(latitude)$, a', b', u', v' are the perturbation longitudinal and latitudinal magnetic fields and velocities respectively.

We see from Equation (2) that the change in differential rotation, $\partial\omega_0/\partial t$, will be greatest where the Reynolds and/or Maxwell stresses change most rapidly with latitude. Equation (2) is for strictly 2D disturbances, but a similar formula, with some relatively minor additional terms, applies in the so-called 'shallow water' case (Dikpati and Gilman, 2001a; Gilman and Dikpati, 2002; Dikpati, Gilman, and Rempel, 2003).

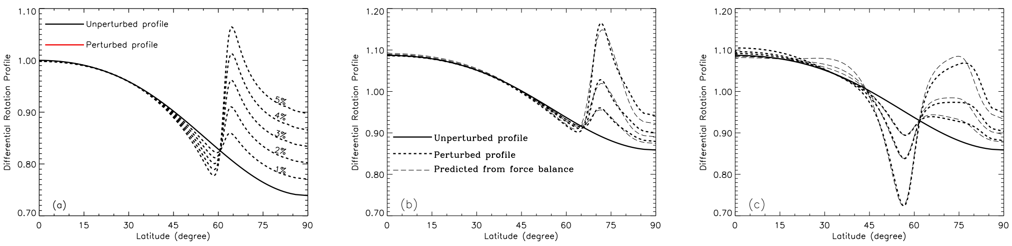

Figure 3. Left panel presents initial jet from linear theory in a 2D hydrodynamic tachocline; middle and right panels respectively present jets in a radiative and overshoot tachocline in a shallow-water model.

To evaluate Equation (2) using linear exponentially growing unstable solutions from the various calculations referenced above, we must assign a disturbance amplitude arbitrarily. Figure 3 shows three representative differential rotation profiles that result from doing that. The profile on the left is for the strictly 2D hydrodynamical case, taken from Charbonneau, Dikpati and Gilman (1999). The two profiles on the right are taken from the shallow water hydrodynamical model of Dikpati and Gilman (2001a) for cases with 'effective gravity' characteristic of the radiative tachocline (middle panel) and overshoot tachocline (right panel).

The primary message from Figure 3 is that, although the details differ, all three cases show the development of a prograde jet at latitudes above about 60° as a result of the global hydrodynamic instability of differential rotation characteristic of the tachocline. Thus if the hydrodynamic form of the global instability is excited in the tachocline, we should expect to see high latitude nonmigrating jets.

Figure 4 generated from a new nonlinear shallow water model of Dikpati (2005), verifies that such jets will reach significant amplitude before being bounded by nonlinearities of the system. In Figure 4 we see a simulation of the development to finite amplitude of high latitude jets, in ~ 1 month, with this model, compared to initial differential rotation profile that has no jet.

Figure 5, taken from nonlinear 2D MHD calculations of Cally, Dikpati and Gilman (2004), shows that jets are excited also in the MHD case, but these

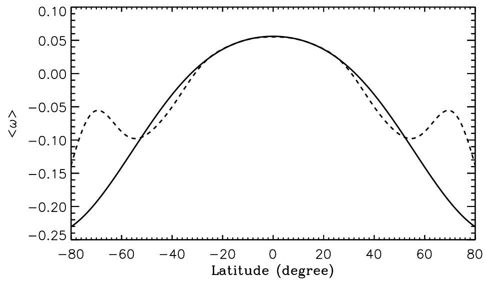

Figure 4. Hydrodynamic jet from nonlinear theory in a shallow-water model of solar tachocline.

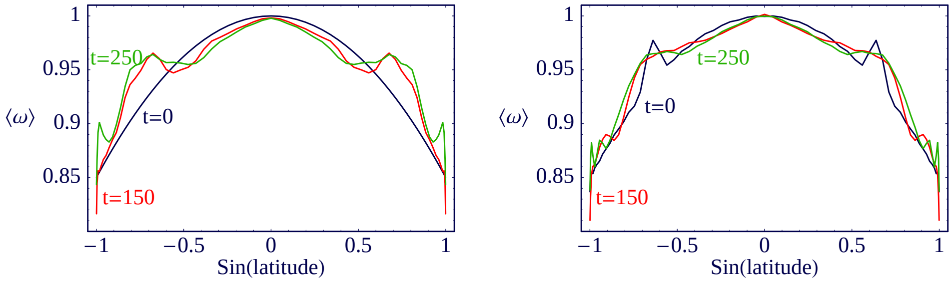

Figure 5. MHD jets from nonlinear theory in a 2D MHD solar tachocline.

occur in the neighborhood of the initial location of a strong toroidal band in the tachocline, in the case shown a 100kG band placed at latitude 40°. Here the jet acquires some of the properties of the equilibrium profile discussed in §2.1, but the jet is only about 20% of the maximum possible, if Coriolis forces entirely balance the poleward directed curvature stress. If the toroidal band is placed initially at a different latitude, the resulting jet will also occur at that latitude. For this MHD case, the primary creator of the jet is the convergence of the Maxwell stress, while in the hydrodynamical cases described above, the primary jet creator is the convergence of the Reynolds stress (see equation 2).

It follows that in the sun, with a dynamo creating new toroidal field closer and closer to the equator as the cycle progresses, a possible global MHD instability would create a jet located with the peak toroidal field and migrating equatorward with it. But if instead the global hydrodynamic instability is active, then we expect it to create high-latitude jets (one in each hemisphere) that do not migrate toward the equator.

A remaining issue is whether it is possible for the hydrodynamic instability to be active in the solar tachocline if it contains toroidal fields of peak amplitude $\sim$100kG. The answer depends critically upon how narrow the toroidal field profile is, and at what latitude it peaks. It is clear from Gilman and Fox (1997), Dikpati and Gilman (1999), and Gilman and Dikpati (2002) that for broad toroidal field profiles, which largely fill the domain between equator and pole in each hemisphere, and have peak fields of $\sim$ 100kG, no hydrodynamic instability is possible.

On the other hand, Dikpati, Gilman and Rempel (2003) showed that hydrodynamic instability could occur for toroidal bands of 10° width in latitude, provided the band was closer to the equator than about 10°. In that case the toroidal band essentially acts as a low-latitude barrier, and the hydrodynamicly unstable modes fill the entire range of latitudes poleward of the band.

Given the helioseismic results for jets that we report below, we have returned to the MHD shallow water system and explored more systematically under what conditions the hydrodynamic instability could occur, as a function of toroidal band width and latitude location. The details of these results will be published elsewhere, but in summary we find that the narrower the band, the higher the latitude the band can be placed at without suppressing the hydrodynamic instability. For bands of 5° width, hydrodynamic instability occurs for all band locations equatorward of about 30° while for a width of 2° this is the case for all band locations equatorward of about 50°.

The reason that the hydrodynamic instability can occur with sufficiently narrow toroidal bands placed at higher latitudes is that narrow bands no longer serve as a true barrier to the perturbations. Instead, close examination of the structure of unstable modes with latitude shows that the perturbations, though larger on the poleward side, are 'tunnelling' through the toroidal band to join with a hydrodynamic disturbance on the other side.

Thus if the toroidal band is narrow enough, the hydrodynamic instability could occur in the solar tachocline for almost all phases of the solar cycle. Thus the existence of persistent stationary high-latitude jets in the solar tachocline could tell us something about the width of the toroidal band as well as the range of latitudes where the band could be found.

3. Helioseismic search for jets

Helioseismology has provided detailed information on the solar internal rotation; for reviews, see for example Christensen-Dalsgaard (2002) and Thompson et al. (2003). Particularly valuable for the present investigation are the long homogeneous series of observations obtained with the GONG network and the MDI instrument on the SOHO spacecraft. The present analysis is based on data from GONG. They were available in overlapping segments of length three 'GONG months', i.e., 108 days, with starting times separated by one GONG month, over the period 1996 – 2003.

3.1. Inversion methods

An overview of inversion techniques was provided by Schou et al. (1998). The data are provided in the form of the so-called a coefficients $a_k(n,l)$, obtained from a polynomial expansion of the rotationally induced frequency splitting according to azimuthal order m, for each radial order n and degree l. These are related to the solar internal angular velocity $\Omega(r,\theta)$, as a function of distance r to the centre and co-latitude θ by

$$a_i \equiv a_k(n,l) = \frac{1}{2\pi}\int_0^R \int_0^\pi K_i(r,\theta)\Omega(r,\theta) r \mathrm{d}r \mathrm{d}\theta \ , \tag{3}$$

where i represents nlk. The *kernels* K_i are determined from the oscillation eigenfunctions for a model of solar structure, which can be regarded as known with sufficient accuracy given helioseismic inferences.

For the inversion methods considered here the inferred rotation rate at some point (r_0, θ_0) can be represented as

$$\bar{\Omega}(r_0, \theta_0) = \sum_i c_i(r_0, \theta_0) a_i = \int_0^R \int_0^\pi \mathcal{K}(r_0, \theta_0; r, \theta) \Omega(r, \theta) r \mathrm{d}r \mathrm{d}\theta \; , \tag{4}$$

where the second representation follows from the first by using equation (3). The *averaging kernel* $\mathcal{K}$ is typically normalized to have unit integral over r and θ, such that equation (4) provides $\bar{\Omega}$ as a weighted average of the true angular velocity. The resolution of the inference is obviously determined by the properties of $\mathcal{K}$. The error properties of the inference can be obtained from the *inversion coefficients* c_i: if, for example, the data a_i are assumed to be independent and with standard deviations σ_i, the standard deviation $\sigma[\bar{\Omega}(r_0, \theta_0)]$ is given by

$$\sigma[\bar{\Omega}(r_0, \theta_0)]^2 = \sum_i c_i(r_0, \theta_0)^2 \sigma_i^2 \; . \tag{5}$$

It is important to keep in mind that even if the data may be independent, the inferences at neighboring points (r_0, θ_0) are generally strongly correlated, since they are based on essentially the same data a_i. The characteristic extent in (r_0, θ_0) of this correlation is typically similar to the extent of the averaging kernel $\mathcal{K}$ (e.g. Howe & Thompson 1996, Larsen et al. 1998, Howe et al. 2000).

The details of the inversion methods lie in the way the inversion coefficients are determined. In one class of techniques, the so-called optimally-localized averaged (OLA) techniques, the c_i are determined explicitly such that the averaging kernels are localized as far as possible near the target location (r_0, θ_0), while controlling the error in the inference. For regularized least-squares (RLS) inversion, a parametrized representation of the solution is determined through a least-squares fit, regularized by minimizing at the same time some measure of the properties of the solution; in the present application a measure of the square of the second derivative has been used, thus restricting rapid variations in the solution. This also serves to limit the error in the inference. The inversion coefficients, and hence the averaging kernels and standard deviations, can be obtained as a result of this fit.

3.2. Differencing inversion solutions

The principal product of a rotation inversion is the solution, which shows a representation of the sun's internal rotation as a function of position. A localized jet may not stand out in the solution, however, unless its amplitude is much larger than the contrast of differential rotation in that region of the sun. Therefore, in order better to reveal jets that may be changing in amplitude or position over time, we take differences between solutions at different epochs.

3.3. Results

We search for persistent or moving features in the tachocline region by considering differences between individual 108-day inferences or yearly averages and a reference provided by the average rotation rate for 1996, near solar minimum. Standard deviations for the averages are evaluated taking into account the correlation between the partly overlapping data series.

In Figure 6 the first two panels show the average and standard error for 1996, obtained with the OLA technique. The average shows the now familiar pattern of latitudinal differential rotation in the convection zone and nearly uniform rotation in the radiative interior, the transition taking place in a thin tachocline. The error plot shows that the inferred standard error is fairly uniform in the relevant region; typical errors in the yearly average are between 2 and 3 nHz, the errors for the individual 108-day series being larger by a factor of around 1.7.

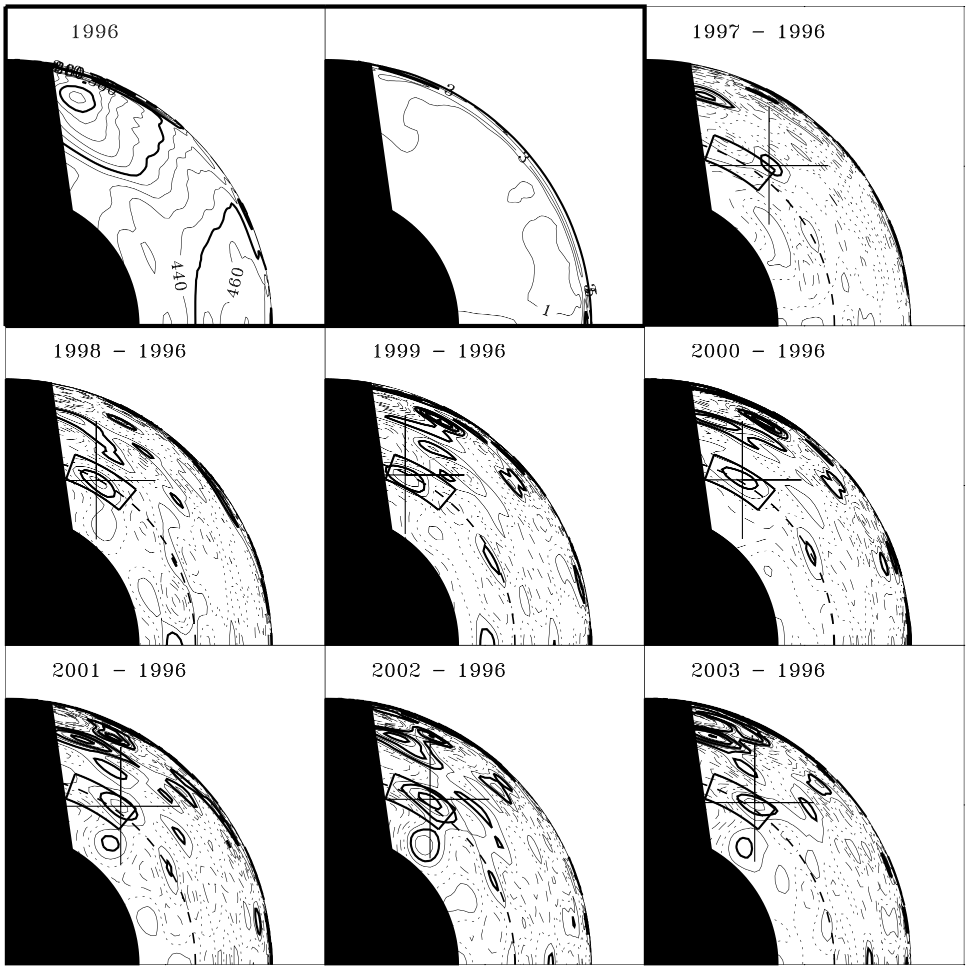

Figure 6. Extreme upper left panel represents OLA rotation rate for 1996; contour spacing 10 nHz; center panel top row, error contours for same. All following panels are differences in rotation between the year indicated, and 1996.

The remaining panels show differences between yearly averages for 1997 – 2003, and the yearly average for 1996. Beginning around 1998 a localized enhancement, or jet-like feature, is visible at high latitudes in the tachocline region, apparently growing in strength until 2002. The extent of the feature is essentially consistent with the extent of the averaging kernel or error correlation at this location. Thus only upper limits on the actual extent of a corresponding true solar feature can be determined. Also, it should be noticed that due to error correlation even random errors in the data would produce features of similar extent, as are indeed seen elsewhere in the difference plots. However, the present feature has an amplitude of several standard deviations (see also Fig. 8 below); this property, and the approximately fixed location of the feature, suggests that it may be real.

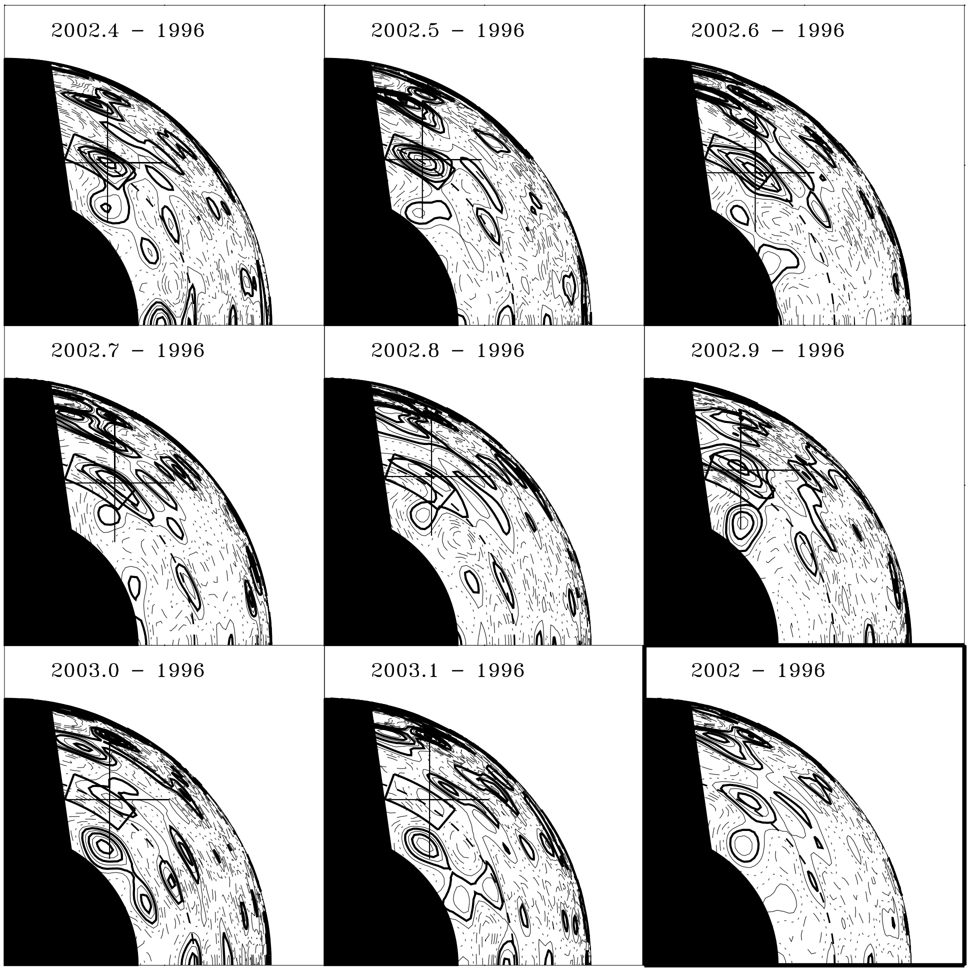

Figure 7. Similar to Figure 6, except for 3 GONG month intervals (108 days), centered on the month indicated (e.g. 2002.4 is the 4th GONG month in 2002).

This conclusion is strengthened by Figure 7, which shows differences for individual 108-day time series in 2002, the year of the largest average jet signal. Due to the overlap between the data series successive groups of three inferences are somewhat correlated; however, even taking this into account the feature seems to be consistently present throughout the year, although weakening towards the end.

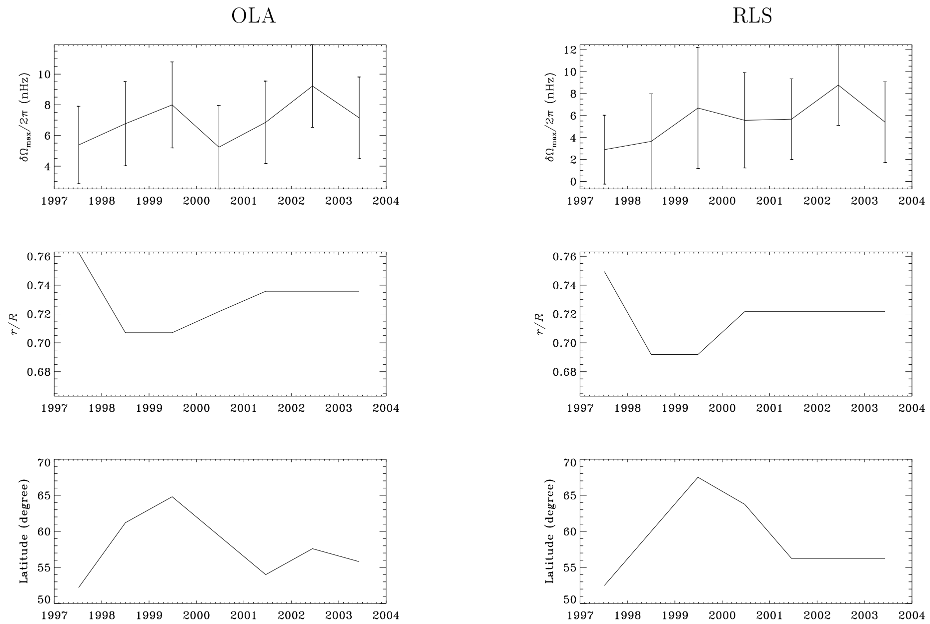

Figure 8. Top row: residual rotation signal found in the jet (relative to the year 1996). Middle row: radial location of the jet in each year. Bottom row: Latitudinal location of the jet.

To provide a clearer impression of the jet and its potential dependence on the inversion method Fig. 8 shows its maximum amplitude, with 1-σ error bars, and location for the yearly averages as determined both with the OLA and RLS techniques. This was determined from the maximum of the difference in a box of extent $0.1R$ in radius and centered on the base of the convection zone, at $r = 0.713R$, and extending between latitude 50° and 70°; the box is indicated in Figs 6 and 7, where also the located maxima are shown by crosses The maximum difference in the jet is clearly significant at the $1 - 2\ \sigma$ level, and there is essentially consistency between the two methods in the temporal variation and location of the maximum. Also, it is clear that the jet is essentially stationary, with a radial location very close to the base of the convection zone.

4. Comments and conclusions

Our principal conclusion is that we have found observational evidence of persistent prograde high latitude jets of fluid (one in each hemisphere) in the solar tachocline throughout most of a solar cycle. However, we are unable to find evidence of jets migrating toward the equator with the advancing phase of the solar cycle. These findings support the prediction of jets in the tachocline caused by a hydrodynamic instability of the latitudinal differential rotation there, and do not support the concept of prograde jets associated with bands of toroidal fields responsible for the appearance of sunspots.

Confidence in our observational finding is bolstered by the fact that two different helioseismic methods (OLA and RLS) give basically similar results, and by the fact that the jets are detectable in 108 day sequences of data as well as annual data, though with greater noise present. Nevertheless, our results should be considered preliminary and in need of verification with other data and methods in the future.

Our results imply that the latitudinal force balance, required to prevent strong toroidal rings from slipping toward the poles due to the magnetic curvature stress, must come primarily from latitudinal pressure gradients than from coriolis forces.

The fact that high latitude jets are found at almost all phases of a solar cycle implies that toroidal fields, likely to be almost always present in the solar tachocline due to dynamo action, must not be strong enough in amplitude or broad enough in latitude profile to interfere with the hydrodynamic instability there. Two of us (Dikpati and Gilman) are exploring in detail what restrictions this inference places on the toroidal field, but we can say that toroidal fields of magnitude $\sim$100kG should be confined to sunspot latitudes and not be broader than $\sim 5^\circ$ in latitude.

Acknowledgments. We acknowledge the support from NASA through the awards W-10107 and W-10175.

References

Cally, P. S., Dikpati, M. & Gilman, P. A., 1999. *Highlights of Astronomy, IAU 2004*, eds. O. Engvold, (in press).

Charbonneau, P., Dikpati, M. & Gilman, P. A., 1999. *Astrophys. J.*, **526**, 523 – 537.

Christensen-Dalsgaard, J., 2002. *Rev. Mod. Phys.*, **74**, 1073 – 1129.

Dikpati, M. & Gilman, P. A., 1999. *Astrophys. J.*, **512**, 417 – 441.

Dikpati, M. & Gilman, P. A., 2001a. *Astrophys. J.*, **551**, 536 – 564.

Dikpati, M. & Gilman, P. A., 2001b. *Astrophys. J.*, **552**, 348 – 353.

Dikpati, M., Gilman, P. A. & Rempel, M., 2003. *Astrophys. J.*, **596**, 680 – 697.

Gilman, P. A. & Fox, P. A., 1997. *Astrophys. J.*, **484**, 439 – 454.

Gilman, P. A. & Dikpati, M., 2002. *Astrophys. J.*, **576**, 1031 – 1047.

Howe, R. & Thompson, M. J., 1996. *Mon. Not. R. astr. Soc.*, **281**, 1385 – 1392.

Howe, R., Christensen-Dalsgaard, J., Hill, F., Komm, R. W., Larsen, R. M., Schou, J., Thompson, M. J. & Toomre, J., 2000. *Science*, **287**, 2456 – 2460.

Larsen, R. M., Christensen-Dalsgaard, J., Kosovichev, A. G. & Schou, J., 1998. In *Structure and dynamics of the interior of the Sun and Sun-like stars; Proc. SOHO 6/GONG 98 Workshop*, eds S.G. Korzennik & A. Wilson, ESA SP-418, ESA Publications Division, Noordwijk, The Netherlands, p. 813 – 818.

Rempel, M. & Dikpati, M., 2002. *Astrophys. J.*, **584**, 524 – 527.

Schou, J., Antia, H. M., Basu, S., Bogart, R. S., Bush, R. I., Chitre, S. M., Christensen-Dalsgaard, J., Di Mauro, M. P., Dziembowski, W. A., Eff-Darwich, A., Gough, D. O., Haber, D. A., Hoeksema, J. T., Howe, R., Korzennik, S. G., Kosovichev, A. G., Larsen, R. M., Pijpers, F. P., Scherrer, P. H., Sekii, T., Tarbell, T. D., Title, A. M., Thompson, M. J., Toomre, J., 1998. *Astrophys. J.*, **505**, 390 – 417.

Thompson, M. J., Christensen-Dalsgaard, J., Miesch, M. S. & Toomre, J., 2003. *Annu. Rev. Astron. Astrophys.*, **41**, 599 – 643.